



HAL
open science

CARD9 in Neutrophils Protects from Colitis and Controls Mitochondrial Metabolism and Cell Survival

Camille Danne, Chloé Michaudel, Jurate Skerniskyte, Julien Planchais, Aurélie Magniez, Allison Agus, Marie Laure Michel, Bruno Lamas, Gregory Da Costa, Madeleine Spatz, et al.

► **To cite this version:**

Camille Danne, Chloé Michaudel, Jurate Skerniskyte, Julien Planchais, Aurélie Magniez, et al.. CARD9 in Neutrophils Protects from Colitis and Controls Mitochondrial Metabolism and Cell Survival. 2022. hal-03791244v1

HAL Id: hal-03791244

<https://ut3-toulouseinp.hal.science/hal-03791244v1>

Preprint submitted on 9 Sep 2022 (v1), last revised 3 Oct 2022 (v2)

HAL is a multi-disciplinary open access archive for the deposit and dissemination of scientific research documents, whether they are published or not. The documents may come from teaching and research institutions in France or abroad, or from public or private research centers.

L'archive ouverte pluridisciplinaire **HAL**, est destinée au dépôt et à la diffusion de documents scientifiques de niveau recherche, publiés ou non, émanant des établissements d'enseignement et de recherche français ou étrangers, des laboratoires publics ou privés.

Copyright

1 **CARD9 in Neutrophils Protects from Colitis**
2 **and Controls Mitochondrial Metabolism and Cell Survival**

3

4 Camille Danne^{1,2,3*}, Chloé Michaudel^{1,3}, Jurate Skerniskyte⁴, Julien Planchais^{1,3}, Aurélie Magniez^{1,3},
5 Allison Agus^{1,3}, Marie-Laure Michel^{1,3}, Bruno Lamas^{1,3}, Gregory Da-Costa^{1,3}, Madeleine Spatz^{1,3},
6 Cyriane Oeuvray^{2,3}, Chloé Galbert^{2,3}, Maxime Poirier^{1,3}, Yazhou Wang^{1,3}, Alexia Lapierre^{1,3}, Nathalie
7 Rolhion^{2,3}, Tatiana Ledent², Cédric Pionneau⁵, Solenne Chardonnet⁵, Floriant Bellvert⁶, Edern
8 Cahoreau⁶, Amandine Rocher⁶, Rafael Jose Argüello⁷, Carole Peyssonnaud⁸, Sabine Louis⁸, Mathias
9 L.-Richard^{1,3}, Philippe Langella^{1,3}, Jamel El-Benna⁹, Benoit Marteyn^{4,10,11}, Harry Sokol^{1,2,3*}

10

11 ¹ Université Paris-Saclay, INRAE, AgroParisTech, Micalis Institute, Jouy-en-Josas, France

12 ² Sorbonne Université, INSERM UMRS-938, Centre de Recherche Saint-Antoine, CRSA, AP-HP,
13 Hôpital Saint-Antoine, Service de Gastroentérologie, F-75012 Paris, France

14 ³ Paris Center for Microbiome Medicine (PaCeMM) FHU, Paris, France

15 ⁴ CNRS, UPR 9002, Université de Strasbourg, Institut de Biologie Moléculaire et Cellulaire,
16 Architecture et Réactivité de l'ARN, Strasbourg, France

17 ⁵ Sorbonne Université, Inserm, UMS PASS, Plateforme Post-génomique de la Pitié Salpêtrière (P3S),
18 Paris, France

19 ⁶ MetaToul-MetaboHUB, National Infrastructure of Metabolomics & Fluxomics (ANR-11-INBS-0010),
20 31077 Toulouse, France

21 ⁷ Aix Marseille Univ, CNRS, INSERM, CIML, Centre d'Immunologie de Marseille-Luminy, Marseille,
22 France

23 ⁸ Institut Cochin, Inserm, CNRS, Université de Paris, Laboratoire d'excellence GR-Ex, Paris, France

24 ⁹ Université de Paris, INSERM-U1149, CNRS-ERL8252, Centre de Recherche sur l'Inflammation
25 (CRI), Laboratoire d'Excellence Inflammex, Faculté de Médecine Xavier Bichat, Paris, France

26 ¹⁰ University of Strasbourg Institute for Advanced Study (USIAS), Strasbourg, France

27 ¹¹ Institut Pasteur, Université de Paris, Inserm 1225 Unité de Pathogénèse des Infections Vasculaires,
28 28 rue du Dr. Roux, 75724 Paris Cedex 15, France

29

30 *Co-Corresponding Authors: Camille Danne, PhD, Centre de Recherche Saint-Antoine, 27 rue
31 Chaligny, 75012 Paris, France (camille.danne@gmail.com) and Harry Sokol, MD, PhD, Service de
32 Gastro-entérologie, Hôpital Saint-Antoine, 184 rue du Faubourg Saint-Antoine, 75571 Paris Cedex 12,
33 France (harry.sokol@aphp.fr).

34

35

36 **Words count** : ~4500 (including material & methods)

37 **Keywords** : IBD, gut inflammation, CARD9, neutrophils, apoptosis, mitochondrial activity

38

39

40 **ABSTRACT**

41 **Objectives** : Inflammatory bowel disease (IBD) results from a combination of genetic predisposition,
42 dysbiosis of the gut microbiota and environmental factors, leading to alterations in the gastrointestinal
43 immune response and chronic inflammation. Caspase recruitment domain 9 (*Card9*), one of the IBD
44 susceptibility genes, has been shown to protect against intestinal inflammation and fungal infection.
45 However, the cell types and mechanisms involved in the CARD9 protective role against inflammation
46 remain unknown.

47 **Design** : We used dextran sulfate sodium (DSS)-induced and adoptive transfer colitis models in total
48 and conditional CARD9 knock-out mice to uncover which cell types play a role in the CARD9
49 protective phenotype. The impact of *Card9* deletion on neutrophil function was assessed by an *in vivo*
50 model of fungal infection and various functional assays, including endpoint dilution assay, apoptosis
51 assay by flow cytometry, proteomics and real time bioenergetic profile analysis (Seahorse).

52 **Results** : Lymphocytes are not intrinsically involved in the CARD9 protective role against colitis.
53 CARD9 expression in neutrophils, but not in epithelial or CD11c+ cells, protects against DSS-induced

54 colitis. In the absence of CARD9, mitochondrial dysfunction in neutrophils leads to their premature
55 death through apoptosis, especially in oxidative environment. The decrease of functional neutrophils in
56 tissues could explain the impaired containment of fungi and increased susceptibility to intestinal
57 inflammation.

58 **Conclusion** : These results provide new insight into the role of CARD9 in neutrophil mitochondrial
59 function and its involvement in intestinal inflammation, paving the way for new therapeutic strategies
60 targeting neutrophils.

61

62

63 **Summary box**

64 **1. What is already known about this subject?**

- 65 • Inflammatory bowel disease (IBD) results from genetic predisposition, microbiota dysbiosis
66 and environmental factors, but the alterations of the immune response leading to chronic
67 intestinal inflammation are still not fully understood.
- 68 • Caspase recruitment domain 9 (*Card9*), one of the IBD susceptibility genes, has been shown
69 to protect against intestinal inflammation and fungal infection.
- 70 • However, the cell types and cellular mechanisms involved in the CARD9 protective role
71 against inflammation remain unknown.

72 **2. What are the new findings?**

- 73 • CARD9 expression in neutrophils, but not in lymphocytes, epithelial cells or CD11c+ cells,
74 protects against DSS-induced colitis.
- 75 • In the absence of CARD9, mitochondrial dysfunction in neutrophils leads to their premature
76 death through apoptosis, especially in oxidative environment.
- 77 • The decrease of functional neutrophils in tissues could explain the impaired containment of
78 fungi and increased susceptibility to intestinal inflammation.

79 **3. How might it impact on clinical practice in the foreseeable future?**

- 80 • These results provide new insight into the role of CARD9 in neutrophil mitochondrial function
81 and its involvement in intestinal inflammation.
- 82 • Understanding the role of neutrophils in chronic inflammation could lead to innovative
83 therapeutic strategies targeting these key immune cells for various complex diseases.

84

85 INTRODUCTION

86 Inflammatory bowel disease (IBD) results from a combination of genetic predisposition,
87 dysbiosis of the gut microbiota and environmental factors, leading to alterations in the gastrointestinal
88 immune response and chronic inflammation^{1,2}. Especially, the innate compartment of the immune
89 system has been involved in IBD development, with a role for dendritic cells, macrophages and
90 neutrophils³⁻⁶. Neutrophils, one of the most abundant and important mediators of innate immunity, are
91 professional phagocytes that mount the acute inflammatory response and act as the first line of
92 defense against invading pathogens^{7,8}. An impaired neutrophil function may result in limited pathogen
93 clearance and fuel a chronic inflammatory response with excessive lymphocyte activation. Patients
94 with congenital disorders in neutrophil function such as chronic granulomatous disease (CGD) often
95 develop IBD-like phenotypes⁹⁻¹². Moreover, functional defects have been observed in neutrophils from
96 IBD patients, including impaired chemotaxis, migration, phagocytosis or ROS production^{4,5}.

97 CARD9, one of the numerous IBD susceptibility genes, encodes an adaptor protein that
98 integrates signals downstream of pattern recognition receptors¹³⁻¹⁸. Especially, CARD9 is involved in
99 the host defense against fungi via C-type lectin sensing^{19,20}. CARD9 polymorphisms in humans are
100 associated with multiple susceptibilities including IBD²¹, whereas loss-of-function mutations are
101 associated with invasive fungal infections caused by species such as *Candida albicans*²¹⁻²⁴. CARD9
102 was shown to mediate its protective functions, at least in part, through the induction of adaptive Th17
103 cell responses^{22,23,25}. *Card9*^{-/-} mice are more susceptible to colitis due to impaired IL-22 production
104 and have an increased load of gut-resident fungi²⁵. Indeed, CARD9 affects the composition and
105 function of the gut microbiota, altering the production of anti-inflammatory microbial metabolites^{26,27}.
106 However, the cell types involved in the CARD9 protective role against intestinal inflammation remain
107 unknown.

108 In this work, we show that CARD9 expression in neutrophils, but not in epithelial or CD11c+
109 cells such as dendritic cells, protects against dextran sulfate sodium (DSS)-induced colitis in mice.
110 The absence of CARD9 impacts neutrophil capacity to contain fungal dissemination, notably by
111 impairing neutrophil mitochondrial function and survival. Indeed, *Card9* deletion induces a basal
112 overactivation of mitochondria, increasing mitochondrial dysfunction and apoptosis in neutrophils.

113 These results provide new insight into the role of CARD9 in neutrophil mitochondrial function and its
114 consequences in intestinal inflammation.

115

116 RESULTS

117 Lymphocytes have no intrinsic role in the *Card9*^{-/-} susceptibility to colitis

118 CARD9 was previously reported to be mainly expressed in myeloid cells, especially dendritic
119 cells, macrophages and neutrophils^{14,28}. Using qRT-PCR analyses in various C57BL/6 mouse organs,
120 we confirmed that *Card9* is mainly expressed in immune organs such as bone marrow, spleen and
121 distal small intestine (ileum), but is low at baseline in proximal and mid small intestine, caecum, colon,
122 stomach and liver, and not detectable in *Card9*^{-/-} tissues (Fig. S1A). Consistently, western-blot analysis
123 showed the expression of CARD9 protein in bone marrow, spleen and distal small intestine of WT
124 mice (Fig. S1B). To dissect *Card9* expression at the cellular level, we sorted immune cell populations
125 from spleen and bone marrow of WT mice. *Card9* is highly expressed in neutrophils (Ly6G⁺CD11b⁺
126 cells), macrophages (CD11b⁺F4/80⁺ cells), CD11c⁺ cells, including dendritic cells, and monocytes
127 (CD11b^{hi}F4/80⁺ cells); but the expression is lower in innate or adaptive lymphocytes (CD3⁺TCRγδ⁺
128 lymphoid cells, CD3⁺CD4⁺ and CD3⁺CD8⁺ T cells, CD3⁻CD19⁺ B cells) (Fig. S1C). Thus, CARD9 likely
129 plays a major role within the myeloid immune compartment.

130 Previous studies from our group and others started to investigate the role of *Card9* in murine
131 models of experimental colitis, showing that *Card9* deletion increases colitis susceptibility^{25,26,29}. In
132 order to decipher the respective roles of lymphocytes and myeloid cells in the *Card9* susceptibility to
133 intestinal injury and inflammation, we first induced colitis with DSS in *Rag2*^{-/-} and *Rag2*^{-/-}*xCard9*^{-/-} mice
134 that are deficient in functional T and B cells. Mice were euthanized after receiving 3% DSS in drinking
135 water for 7d, as the severity limit was reached for the *Rag2*^{-/-}*xCard9*^{-/-} group. Indeed, disease severity
136 (defined by weight loss, DAI (Disease Activity Index) score, colon length, and histologic score) was
137 strongly increased in *Rag2*^{-/-}*xCard9*^{-/-} mice compared to *Rag2*^{-/-} mice (Fig. 1A-E). In an adoptive
138 transfer model of colitis, in which *Rag2*^{-/-} mice lacking functional lymphocytes received T cells either
139 from WT or *Card9*^{-/-} mice, no difference was observed on colitis severity (Fig. 1F), meaning that *Card9*
140 expression in T cells does not impact colitis susceptibility. However, the transfer of WT T cells into
141 *Rag2*^{-/-}*xCard9*^{-/-} recipient mice did aggravate colitis compared to *Rag2*^{-/-} simple KO recipients, with a

142 significantly stronger weight loss (Fig. 1F). These results demonstrate that *Card9* mediates its
143 protective role against colitis through the innate immunity compartment, although its role in intestinal
144 epithelial cells cannot be ruled out.

145

146 ***Card9* expression in neutrophils, but not in epithelial or CD11c⁺ cells, protects against colitis**

147 Based on these findings, we generated conditional KO mice using the cre-lox technology, and
148 obtained mouse strains defective for *Card9* either in epithelial cells only (Villin^{cre}*Card9*^{lox} line),
149 CD11c-expressing cells only, including dendritic cells, macrophages and monocytes
150 (CD11c^{cre}*Card9*^{lox} line), or neutrophils only (Mrp8^{cre}*Card9*^{lox} line). To validate their phenotypes,
151 we isolated epithelial cells from the colonic lamina propria of *Card9*<sup>Villin^{cre} and *Card9*<sup>Villin^{wt} mice, or used
152 MACS separation columns to isolate either CD11c⁺ or Ly6G⁺ cell fractions from spleen or bone marrow
153 of *Card9*<sup>CD11c^{wt} and *Card9*<sup>CD11c^{cre} mice or *Card9*<sup>Mrp8^{wt} and *Card9*<sup>Mrp8^{cre} mice, respectively. We
154 performed qRT-PCR on these cell fractions (Fig. S2A), and western-blot analyses on the Ly6G⁺ and
155 Ly6G^{low/-} fractions of *Card9*^{WT}, *Card9*^{-/-}, *Card9*<sup>Mrp8^{wt} and *Card9*<sup>Mrp8^{cre} mice (Fig. S2B). Results
156 confirmed that *Card9* deletion is restricted to the expected cell types (Fig. S2A-B). Purity of
157 Ly6G⁺CD11b⁺ neutrophils isolated from the bone marrow of C57Bl/6 mice reached 95% by flow
158 cytometry (Fig. S2C).</sup></sup></sup></sup></sup></sup></sup></sup>

159 We then assessed the susceptibility of these newly generated mice strains in a model of
160 intestinal inflammation. DSS was administered for 7 days, followed by additional 5 days in which DSS
161 was discontinued. The deletion of *Card9* in epithelial or CD11c⁺ cells did not affect mouse
162 susceptibility to colitis (Fig. 2A-B and S2D). However, the deletion of *Card9* in neutrophils aggravates
163 colitis compared to WT littermate controls, with significantly increased weight loss from day 8 (Fig.
164 2C), DAI score from day 5 (Fig. 2C), and histological score (Fig. 2E-F), as well as decreased colon
165 length (Fig. 2D). Thus, the expression of *Card9* in neutrophils plays a crucial role in the protection
166 against intestinal inflammation. The expression of myeloperoxidase (MPO), an anti-microbial enzyme
167 abundantly expressed in neutrophils, was increased in *Card9*<sup>Mrp8^{cre} compared to *Card9*<sup>Mrp8^{wt} colon
168 tissue at day 12, indicating a more important presence or activation of neutrophils in the absence of
169 *Card9* (Fig. 2G). Similarly, the expression of the inflammatory marker lipocalin (*Lcn2*) was increased in
170 *Card9*^{Mrp8^{cre} colon tissue at day 12 (Fig. 2H).}</sup></sup>

171 These results suggest that *Card9*-deficient neutrophils are efficiently recruited to the inflamed
172 tissue but likely exhibit functional defects preventing them from adequately controlling microbial
173 invaders and thus maintaining inflammation within the intestinal mucosa. We previously showed that
174 the gut microbiota of total *Card9*^{-/-} KO lineage mice exhibit an altered production of AhR agonists
175 compared to WT²⁶. However, no difference was observed between *Card9*^{Mrp8wt} and *Card9*^{Mrp8cre} mice
176 (Fig. S2E), suggesting that this aspect of the phenotype is not intrinsically related to the role of CARD9
177 in neutrophils.

178

179 ***Card9* deletion affects the number of activated neutrophils in the inflamed colon**

180 To investigate neutrophil function in WT mice during DSS-induced inflammation, we analyzed
181 RNA expression of the neutrophil-specific genes *Lcn2*, *Cxcr2* and *S100A8* in colon tissue at days 0, 4,
182 7, 9, 12 and 16 of DSS-induced colitis (Fig. 3A and S2F). The neutrophil recruitment was maximal at
183 day 9, corresponding to the peak of clinical inflammation, and remained high up to day 16 (Fig. 3A).
184 Histological sections of the distal colon confirmed these findings (Fig. 3B). The fact that inflammation
185 was higher in *Card9*^{Mrp8cre} than in *Card9*^{Mrp8wt} mice (Fig. S2E), and that *Lcn2*, *Cxcr2* and *S100a8*
186 expression at day 9 in colon tissue were similar in both genotypes (Fig. 3C) excludes the hypothesis of
187 a defect of neutrophil recruitment in *Card9*^{Mrp8cre} mice. We then examined the immune cell populations
188 recruited to the colon lamina propria (LP) of *Card9*^{Mrp8cre} versus *Card9*^{Mrp8wt} mice at day 9 of colitis.
189 Surprisingly, although the total number of neutrophils was similar in the two genotypes, the percentage
190 and count of mature and activated Ly6G⁺CD11b⁺ neutrophils was decreased in the colon LP of
191 *Card9*^{Mrp8cre} (Fig. 3D-E). Moreover, the expression levels of both Ly6G and CD11b surface proteins,
192 two major neutrophil maturation and activation markers, were significantly reduced in the overall
193 neutrophil population, as shown by decreased MFIs (for Mean Fluorescence Intensity) (Fig. 3F-G).
194 These findings suggest a structural or functional defect in neutrophils deleted for *Card9*.

195

196 ***C. albicans* killing capacities are impacted by *Card9* deletion in neutrophils**

197 To investigate the defect caused by *Card9* deletion in *Card9*^{Mrp8cre} compared to *Card9*^{Mrp8wt}
198 neutrophils, we developed several *in vitro* assays with Ly6G⁺ neutrophils purified from mouse bone

199 marrow using MACS separation columns. Immunofluorescence, scanning electron microscopy (SEM)
200 and transmission electron microscopy (TEM) analyses did not reveal noticeable structural differences
201 between both genotypes (Fig. S3). On the functional side, we tested the neutrophils ability to kill
202 microorganisms, especially fungi, as CARD9 plays a crucial role in host defense against fungal
203 infection in both humans and mice^{25,20}. Indeed, *C. albicans* killing capacities are strongly affected by
204 *Card9* deletion in neutrophils (Fig. 4). An endpoint-dilution survival assay in 96-well plates revealed
205 that twice as many *C. albicans* cfu (colony forming unit) do survive after 24h co-incubation with *Card9*
206 ^{-/-} or *Card9*^{Mrp8^{cre}} neutrophils compared to *Card9*WT or *Card9*^{Mrp8^{wt}} controls, respectively (Fig. 4A-B). A
207 killing assay using the cfu counting method on agar plates confirmed that *Card9*^{Mrp8^{cre}} neutrophils have
208 impaired abilities to kill *C. albicans* compared to *Card9*^{Mrp8^{wt}} (Fig. 4C). *Card9* deletion in neutrophils did
209 not impact phagocytosis *per se*, as shown by flow cytometry experiments using fluorescein-
210 isothiocyanate (FITC)-conjugated zymosan (from *Saccharomyces cerevisiae* cell wall), or cultures of
211 live *C. albicans*-GFP or *E. coli*-GFP (Fig. S4A-B). Moreover, we did not observe a difference in the
212 levels of Reactive Oxygen Species (ROS) production over time between neutrophils of the two
213 genotypes in response to phorbol myristate acetate (PMA), a PKC-dependent neutrophil activator, or
214 zymosan, a fungal stimulus (Fig. S4C-E). Even though *Card9* is involved in autophagy³⁰, this cellular
215 process did not seem to be affected by *Card9* deletion in neutrophils *in vitro*, as shown by the
216 normality of p62 and LC3BII/I ratio on western-blot (Fig. S4F).

217 We thus followed the track of fungal killing to investigate whether the absence of *Card9*
218 expression in neutrophils drives a general impairment of the immune system to control infection.
219 During a DSS-induced colitis model, we detected a slight but non-significant increase in total
220 fungi/bacteria DNA ratio at days 7 and 12 in the feces of *Card9*^{Mrp8^{cre}} compared to *Card9*^{Mrp8^{wt}} mice
221 (Fig. S4G). These data suggest a reduced ability of *Card9*^{Mrp8^{cre}} mice to contain fungi expansion in the
222 inflamed intestine. However, this effect might be difficult to point out due to the very low fungal
223 abundance in SPF mouse microbiota. Thus, to go further and reveal a potential phenotype, we
224 induced colitis in mice treated with a broad-spectrum antibiotic and antifungal cocktail and gavaged
225 with *C. albicans* to expand the intestinal fungal load (Fig. 4D). The increased colitis severity in
226 *Card9*^{Mrp8^{cre}} mice was maintained in this setting (Fig. 4E-G). *C. albicans* load was slightly increased
227 (although not statistically significant) in the caecal content (Fig. 4H-I), colon and caecal tissues (Fig.
228 4J) of *Card9*^{Mrp8^{cre}} mice, and the number of cfu recovered from liver, spleen and kidney were

229 significantly higher compared to *Card9*^{Mrp8wt} mice (Fig. 4K). These results show that *Card9* expression
230 in neutrophils is crucial to control the fungal load in the inflamed gut, the direct translocation of *C.*
231 *albicans* from the gut to the liver, and to avoid its systemic dissemination.

232

233 **The absence of *Card9* impacts neutrophils survival by increasing apoptosis**

234 To explore the mechanisms underlying the impaired capacity of *Card9*^{Mrp8cre} neutrophils to kill
235 *C. albicans* despite intact phagocytosis, autophagy, and ROS production, we investigated neutrophils
236 survival rates by flow cytometry using an AnnexinV-FITC assay coupled to Live/Dead staining (Fig. 5).
237 AnnexinV reveals ongoing apoptosis, whereas Live/Dead only stains permeable dead cells.
238 Interestingly, after 1h incubation at 37°C, *Card9*^{Mrp8cre} neutrophils showed a significant increase in
239 AnnexinV-FITC MFI compared to *Card9*^{Mrp8wt} neutrophils (Fig. 5A-B). Consistently, an increase in
240 percentages of apoptotic (Q1, AnnexinV⁺LD⁻) and dead (late apoptotic/necrotic) neutrophils (Q2,
241 AnnexinV⁺LD⁺), and a decrease in viable neutrophils (Q4, AnnexinV⁻LD⁻), were observed for the
242 *Card9*^{Mrp8cre} genotype (Fig. 5C). Interestingly, the surface expression of the CD62L marker (a surface
243 protein that is lost upon cell activation) was reduced in *Card9*^{Mrp8cre}, with a lower percentage of CD62L⁺
244 cells and a higher percentage of CD62L⁻ cells (Fig. 5D). These results suggest an excessive basal
245 activation of *Card9*^{Mrp8cre} compared to *Card9*^{Mrp8wt} neutrophils. Similar results were obtained with
246 *Card9*^{-/-} versus *Card9*WT neutrophils (Fig. S5A-D), confirming the impact of *Card9* on neutrophil
247 survival.

248 To go further, we performed a proteomic analysis on *Card9*^{Mrp8cre} versus *Card9*^{Mrp8wt}
249 neutrophils after 1h incubation at 37°C. This approach revealed that a large number of proteins related
250 to cellular metabolism pathways were differentially regulated between both genotypes. Indeed, a Gene
251 Ontology (GO) functional analysis showed the enrichment in numerous cellular metabolic processes,
252 both in unstimulated and stimulated conditions, among proteins statistically down- or up-regulated in
253 *Card9*^{Mrp8cre} compared to *Card9*^{Mrp8wt} neutrophils (Fig. 5E and S5E). Especially, we observed a high
254 prevalence of mitochondrial proteins among the differentially regulated candidates between the two
255 genotypes (Fig. 5F), suggesting that neutrophil mitochondrial functions are impacted by the absence
256 of *Card9*.

257

258 **Card9 controls neutrophil survival by affecting mitochondrial function**

259 Subsequently, we analyzed neutrophil mitochondrial function using MitoTracker Green (reflecting
260 mitochondrial mass) and MitoTracker Red (reflecting mitochondrial membrane potential) markers in a
261 flow cytometry assay (Fig. 6A). No difference was observed in terms of MFIs, but we observed a
262 significant increase in the percentage of MitoGreen⁺MitoRed⁻ neutrophils (with dysfunctional or
263 metabolically inactive mitochondria) in the *Card9*^{Mrp8cre} compared to the *Card9*^{Mrp8wt} genotype (Fig. 6A).
264 Tetramethylrhodamine methyl ester (TMRM) assay evaluating the mitochondrial membrane potential
265 confirmed the increase in apoptotic, metabolically stressed cells (TMRM⁻) among *Card9*^{Mrp8cre}
266 neutrophils (Fig. 6B). These results suggest that the survival defect of *Card9*^{Mrp8cre} neutrophils may be
267 due to an altered energetic metabolism. Real-time bioenergetic profile analysis using Seahorse
268 technology showed that *Card9*^{Mrp8cre} neutrophils have a higher basal Oxygen Consumption Rate
269 (OCR) during a cell mito stress assay (Fig. 6C), indicating a higher oxidative phosphorylation activity
270 compared to *Card9*^{Mrp8wt} neutrophils. Basal respiration and ATP production rate were both highly
271 increased in *Card9*^{Mrp8cre} neutrophils (Fig. 6D). Moreover, a Seahorse real-time ATP rate assay
272 demonstrated that *Card9*^{Mrp8cre} neutrophils have an increased mitochondrial ATP (mitoATP) production
273 rate, whereas glycolytic ATP (glycoATP) production rate is only mildly decreased, as shown by the
274 ATP rate index and the energetic map (Fig. 6E). A Seahorse glycolytic rate assay confirmed the
275 moderate decrease of the basal Extracellular Acidification Rate (ECAR) of *Card9*^{Mrp8cre} neutrophils
276 (Fig. S6A). However, metabolomics analysis on neutrophil supernatants incubated for 24h revealed a
277 decreased in lactate production, leading to a reduced lactate/glucose ratio in *Card9*^{Mrp8cre} neutrophils
278 (Fig. S6B). Similar results were obtained when we compared *Card9*^{WT} and *Card9*^{-/-} neutrophils in the
279 assays described above (Fig. S6C-E). Thus, *Card9* deletion in neutrophils induces an overactivation of
280 mitochondria and tends to reduce glycolytic activity, which is the major energy source of normal
281 neutrophils. Blocking glycolysis with 2DG (2-Deoxy-D-glucose) increased the apoptotic rate of
282 *Card9*^{Mrp8wt} but not of *Card9*^{Mrp8cre} neutrophils; showing that glycolysis is more essential to *Card9*^{Mrp8wt}
283 than *Card9*^{Mrp8cre} neutrophils (Fig.6F). Conversely, blocking the mitochondrial respiratory chain with
284 oligomycinA increased the apoptotic rate of *Card9*^{Mrp8cre} but not of *Card9*^{Mrp8wt} neutrophils,
285 demonstrating the crucial role of mitochondria as an energy source in *Card9*^{Mrp8cre} neutrophils (Fig.
286 6G). Thus, contrary to *Card9*^{Mrp8wt} neutrophils that mainly rely on glycolysis as a source of energy,
287 *Card9*^{Mrp8cre} neutrophils present an altered metabolism with an overactivation of mitochondria

288 associated with a dysfunctional state, leading to apoptosis. Intestinal inflammation is associated with a
289 high degree of oxidative stress. To evaluate the effect of oxidative stress on the phenotype of
290 *Card9*^{Mrp8cre} neutrophils, they were treated for 1h with H₂O₂. The increased apoptosis and necrosis
291 rates observed in *Card9*^{Mrp8cre} neutrophils were stronger in oxidative stress than in basal condition
292 (Fig. 6H). These results show that the role of CARD9 in the survival capacity of neutrophils, especially
293 in oxidative conditions, is mediated by effects on mitochondrial functions.

294

295 **DISCUSSION**

296 Altogether, this study reveals that, in the absence of CARD9, mitochondrial dysfunction in
297 neutrophils leads to their premature death through apoptosis, especially in an oxidative environment.
298 The decrease of functional neutrophils in the gut affects fungal containment and increases
299 susceptibility to intestinal inflammation. CARD9 polymorphisms are associated with IBD. Mouse
300 studies showed the contribution of CARD9 to host defense and intestinal barrier, notably through the
301 production of IL-22 and the modulation of the gut microbiota metabolic activity^{25,26}. However, the role
302 of CARD9 in disease pathogenesis has not been elucidated at the cellular level. Our study reveals that
303 *Card9* deletion in neutrophils, contrarily to epithelial or CD11c⁺ cells, increases the susceptibility to
304 DSS-induced colitis. We thus focused on studying the role of CARD9 expression in neutrophil
305 functionality. Indeed, neutrophils have been studied in different models of IBD and fungal infection, but
306 their direct contribution to pathogenesis and the role of CARD9 in these mechanisms remain poorly
307 understood^{31,4,5,32}.

308 Human CARD9 deficiency results in impaired neutrophil fungal killing, leading to a selective
309 defect to contain invasive fungal infection³³. In both humans and mice, CARD9 is required in microglia
310 for neutrophil recruitment and control of fungal infection in the central nervous system^{34,35}. CARD9
311 signaling was also involved in neutrophil phagocytosis and NETosis (Neutrophil extracellular traps)
312 functions, enhancing mouse survival to a lethal dose of *C. albicans*³⁶. Moreover, CARD9 expression in
313 neutrophils promotes autoantibody-induced arthritis and dermatitis in mice³⁷, and inflammation levels
314 in a mouse model of neutrophilic dermatosis³⁸. In line with these studies, we found that *Card9* deletion
315 affects the capacity of neutrophils to kill fungi *in vitro* and *in vivo*, with no impact on neutrophil
316 structure, ROS production, autophagy or phagocytosis. We have not examined the role of CARD9 in

317 chemotaxis because, in the context of fungal infection in patients with CARD9 deficiency, neutrophil-
318 intrinsic chemotaxis was not affected²⁴. In DSS-induced colitis, *Card9* deficiency in neutrophils does
319 not impact their recruitment to the colon, but reduces the number of mature neutrophils. Indeed, we
320 discovered that the absence of CARD9 increases apoptosis rates in neutrophils, and that this
321 premature death was caused by mitochondria overactivation. Indeed, the intrinsic pathway of
322 apoptosis is initiated by the permeabilization of mitochondria, which releases proapoptotic factors into
323 the cytosol^{39,40}. Other CARD proteins mediate apoptotic signaling through CARD-CARD domain
324 interactions¹³. In addition to mediating inflammation, CARD9, a member of the CARD proteins family,
325 was recently shown to inhibit mitochondria-dependent apoptosis of cardiomyocytes under oxidative
326 stress⁴¹. Here, we show that CARD9 also mediates mitochondrial function and apoptosis in
327 neutrophils, especially in an oxidative environment. Further investigation is required to fully elucidate
328 the impact of mitochondria overactivation on neutrophil function, especially *in vivo*. The impact of
329 *Card9* on neutrophil mitochondrial function might not fully explain the increased susceptibility of
330 *Card9*^{Mrp8cre} mice to DSS colitis. Moreover, other cell types are likely involved in the *Card9*^{-/-} mice
331 phenotype, explaining the impact of *Card9* deletion on microbiota metabolic activity, as we show that
332 this is not dependent on neutrophils^{25,26}.

333 Neutrophils contain very few mitochondria compared to other leukocytes, and depend mainly
334 on glycolysis to produce ATP, which is essential to perform their designated tasks. This allows energy
335 generation in a low-oxygen environment and keeps oxygen available for neutrophil effector
336 functions⁴². Thus, the dependence of neutrophils on glycolysis could be an adaptation to allow oxygen
337 to be used in the anti-microbial response rather than entering oxidative phosphorylation⁴². Here, we
338 show that in the absence of CARD9, mitochondria are overactivated in neutrophils, leading to their
339 premature death and the loss of their anti-microbial functions. Alternatively, excessive oxidative
340 phosphorylation could also lead to an overactivation of neutrophils by increasing ATP production,
341 especially in inflammatory environments where their activity is typically tightly controlled by the low
342 oxygen pressure. Neutrophil overactivation could damage the surrounding tissues and exacerbate
343 inflammation, explaining the increased susceptibility to intestinal colitis in the absence of *Card9*. In
344 humans, the « glycogen storage disease type Ib » induces a functional defect of neutrophils due to
345 glycolysis dysfunction and impaired energy homeostasis⁴³. This disease is associated with IBD-like
346 phenotypes, highlighting the importance of neutrophil metabolism in intestinal health^{44,43}.

347 Immunometabolism is a central concept as immunity and metabolism impact each other in both ways :
348 (i) energetic metabolism impacts immune function, which is well-documented for lymphocytes and
349 macrophages⁴⁵, but not for neutrophils; and (ii) we show that a protein known for its roles in innate
350 immunity, CARD9, can also impact cell metabolism. Further investigation is required to understand
351 how CARD9 does interact with mitochondrial function in a direct or indirect manner.

352 Neutrophils are involved in various diseases, including infection, cardiovascular diseases,
353 inflammatory disorders and cancer, which makes them exciting targets for therapeutic intervention⁴⁶.
354 Despite the complex implication of neutrophils in disease, various therapeutic approaches aim to
355 enhance, inhibit or restore neutrophil function, depending on the pathology. In inflammatory diseases
356 with excessive neutrophil activity, their attenuation could be desired, even though killing functions
357 against microorganisms might still need to be preserved. Our work shows that increased apoptosis in
358 neutrophils does not alleviate intestinal inflammation, even though these cells are known to contribute
359 to disease development. Recent studies indicate substantial phenotypic and functional heterogeneity
360 of neutrophils⁴⁶. Thus, targeting a specific subpopulation may allow the attenuation of harmful aspects
361 of neutrophils without compromising host defence. Some neutrophil-targeted therapeutic strategies
362 have reached the clinic, notably in the context of IBD with positive effects of the growth factor
363 granulocyte colony-stimulating factor G-CSF⁴⁷. It opens promising options for numerous complex
364 pathologies.

365

366 **Author Contributions**

367 C.D and H.S. conceived and designed the study, performed data analysis, and wrote the manuscript;
368 C.D. designed and conducted all experiments, unless otherwise indicated; C.M., J.P., A.M., A.A., M.-
369 L.M., B. L., G.D.-C., M.S., C. G., M.P., Y.W., A.L. provided technical help for the *in vitro* and/or *in vivo*
370 experiments; J.S. and B.M. performed the immunofluorescence microscopy experiments; C.Pi. and
371 S.C. conducted the proteomics analyses; F.B., E.C. and A.R. performed the metabolomics analysis;
372 T.L. provided mice and C.O. performed genotyping; C.Pe., S.L. and J.E.-B. helped with ROS
373 production assays; R.J.A provided Scenith kits for tests with neutrophils; C.D., C.M., J.P., M.L.-R.,
374 P.L., N.R., J.E.-B., B. M. and H.S. discussed experiments and results.

375

376 **Acknowledgments**

377 We thank M. Thierry Meylheuc and Ms. Christine Longin from the imaging facility at the microscopy
378 and imaging platform MIMA2 (MIMA2, INRAE, 2018. Microscopy and Imaging Facility for Microbes,
379 Animals and Foods, <https://doi.org/10.15454/1.5572348210007727E12>, Jouy-en-Josas, France) for
380 precious help in SEM and TEM ; the members of the IERP (INRAE) and PHEA (CRSA) animal
381 facilities, and of the @bridge histology platform (Université Paris-Saclay, INRAE, AgroParisTech,
382 GABI) ; and Catherine Brenner for the use of Seahorse XF device (IGR). Thanks to BioRender for the
383 graphical abstract. Funding was provided by the ANR-17-CE15-0019-01 grant and a Marie
384 Skłodowska-Curie Actions fellowship.

385

386 **Declaration of Interests**

387 The authors declare no competing interests.

388

389 **Material and Methods**

390

391 **Mice.** *Card9^{-/-}*, *Rag2^{-/-}xCard9^{-/-}*, *Rag2^{-/-}*, *Card9loxMrp8cre*, *Card9loxVillincre*, and
392 *Card9loxCD11ccre* mice on C57BL/6J background were obtained from the Saint-Antoine Research
393 Center and housed at the IERP (INRAE, Jouy-en-Josas) under specific pathogen-free conditions.
394 Animal experiments were performed according to the institutional guidelines approved by the local
395 ethics committee of the French authorities, the 'Comité d'Ethique en Experimentation Animale'
396 (COMETHEA, CEEA45).

397

398 **Induction of DSS colitis and colonization with *C. albicans*.** Mice were administered drinking water
399 supplemented with 2-3% (wt/vol) DSS (MP Biomedicals) for 5-7 days (depending on colitis severity of
400 each experiment), and then water only for 5d. Animals were monitored daily for weight loss. For *C.*
401 *albicans* colonization, mice were treated with 0.4mg/ml streptomycin, 300U/ml penicillin G and
402 0.125mg/ml fluconazole as indicated on Fig. 4.

403

404 **Histology.** Colon samples were fixed, embedded in paraffin and stained with hematoxylin and eosin.

405 Slides were scanned and analyzed to determine the histological score (Table S1)²⁵.

406

407 **Table S1. Histological grading of colitis**

Feature graded	Grade	Description
Inflammation severity	0	None
	1	Slight
	2	Moderate
	3	Severe
Inflammation extent	0	None
	1	Mucosa
	2	Mucosa and submucosa
	3	Transmural
Crypt damage	0	None
	1	Basal 1/3 damaged
	2	Basal 2/3 damaged
	3	Only surface epithelium lost
	4	Entire crypt and epithelium lost
Percent involvement	1	1-25%
	2	26-50%
	3	51-75%
	4	76-100%

For each feature, the product of the grade and the percentage involvement was established. The histological score was obtained by adding the subscores of each feature.

408

409 **Fecal DNA extraction and total bacteria and fungi quantification.** Fecal DNA was extracted as
410 previously described²⁶. Luna Universal qPCR Master Mix (New England Biolabs) was used for
411 quantification of fungal ITS2 sequences and TaqMan Gene Expression Assays (Life Technologies) for
412 quantification of bacterial 16S rDNA sequences.

413

414 **Cell preparation and stimulation.** Epithelial cells were isolated from colonic tissue using a
415 DTT/EDTA buffer. Neutrophils were purified from mouse bone marrow using anti-Ly6G MicroBeads
416 UltraPure and MACS separation columns (Miltenyi Biotec). CD11c⁺ cells were purified from mouse
417 spleen using anti-CD11c MicroBeads UltraPure and MACS separation columns (Miltenyi Biotec).
418 Purity checks and cell counts were performed using a BD Accuri C6 flow cytometer (BD Biosciences).
419 After purification, neutrophils were seeded in 96-well suspension plate (Sarstedt), rested for 30min in
420 RPMI 1640 Medium (Gibco, ThermoFisher Scientific) before addition of 2% heat-inactivated Fetal
421 Bovine Serum (FBS), 2-DG 10mM, oligomycine 1.5µM or H2O2 0.01M and incubated at 37°C as
422 indicated. Isolation of lamina propria immune cells was performed as previously described⁴⁸.

423

424 **Gene expression analysis using quantitative RT-PCR.** Total RNA was isolated from colon samples
 425 or cell suspensions using RNeasy Mini Kit (Qiagen), and quantitative RT-PCR performed using
 426 QuantiTect Reverse Transcription Kit (Qiagen) and Luna® Universal RT-PCR Kit (New England
 427 Biolabs) in a StepOnePlus apparatus (Applied Biosystems) with specific mouse oligonucleotides
 428 (Table S2). We used the $2^{-\Delta\Delta^{Ct}}$ quantification method with mouse *Gapdh* as an endogenous control
 429 and the WT group as a calibrator.

430

431 **Table S2 List of oligonucleotides and antibodies**

Oligonucleotides	SEQUENCE/SOURCE	IDENTIFIER
<i>Gapdh</i> (sense)	AAC TTT GGC ATT GTG GAA GG	
<i>Gapdh</i> (antisense)	ACA CAT TGG GGG TAG GAA CA	
<i>Card9</i> exon1F (sense)	CAG TGA CCC CAA CCT GGT CAT	
<i>Card9</i> exon3R (antisense)	TCT GCA GCT TCA TGA CCT CTG TC	
All fungi (sense) (ITS1, ITS2)	CTT GGT CAT TTA GAG GAA GTA A	
All fungi (antisense) (ITS1, ITS2)	GCT GCG TTC TTC ATC GAT GC	
All bacteria (sense) (16s)	CGG TGA ATA CGT TCC CGG	
All bacteria (antisense) (16s)	TAC GGC TAC CTT GTT ACG ACT T	
All bacteria (Probe) (16s)	6FAM-CTT GTA CAC ACC GCC CGT C-MGB	
<i>Il-23</i> mouse (sense)	AGC GGG ACA TAT GAA TCT ACT AAG AGA	
<i>Il-23</i> mouse (antisense)	GTC CTA GTA GGG AGG TGT GAA GTT G	
<i>Lcn2</i> mouse	Quantitect	Mn_Lcn2_1_SG QT00113407
<i>Cxcr2</i> mouse (sense)	CTC ACA AAC AGC GTC GTA GAA C	
<i>Cxcr2</i> mouse (antisense)	AGG GCA TGC CAG AGC TAT AAT	
<i>S100a8</i> mouse (sense)	TCA AGA CAT CGT TTG AAA GGA AAT C	
<i>S100a8</i> mouse (antisense)	GGT AGA CAT CAA TGA GGT TGC TC	
Antibodies		
CARD9 (A-8)	Santa Cruz Biotechnology	Cat# sc-374569
β-ACTIN (D6A8)	Cell Signaling Technology	Cat# 8457S
APC-labeled anti-mouse TCRγδ (GL3)	eBioscience	Cat# 17-5711-82
anti-CD16/32 (93)	eBioscience	Cat# 14-0161-85
PerCP5.5-labeled anti-mouse CD45 (30-F11)	eBioscience	Cat# 45-0451-82
FITC-labeled anti-mouse CD3ε (145-2C11)	eBioscience	Cat# 11-0031-85

BV605-labeled anti-mouse CD8 α (53-6.7)	BioLegend	Cat# 100744
PE-labeled anti-mouse CD4 (RM4-5)	eBioscience	Cat# 12-0042-83
AF700-labelled CD19 (6D5)	BioLegend	Cat# 115528
PE-labelled CD11c (N418)	BioLegend	Cat# 117308
APC-labelled F4/80 (BM8)	BioLegend	Cat# 123116
AF700-labelled CD11b (M1/70)	BioLegend	Cat# 101222
APCFire750-labelled CD45 (30-F11)	BioLegend	Cat# 103154
PerCP5.5-labelled Ly6G (1A8)	BioLegend	Cat# 127616
PE-labelled CD11b (M1/70)	eBioscience	Cat# 12-0112-82
BV421-labelled CD62L (MEL-14)	BioLegend	Cat# 104424

432

433 **Immunoblot Analysis.** Mouse tissue or cell suspensions were lysed using Laemmli buffer, loaded on
434 a SDS-PAGE and analyzed with antibodies against CARD9 (A-8:sc-374569, Santa Cruz
435 Biotechnology), or β -ACTIN (D6A8, CST).

436

437 **Flow cytometry, cell sorting and functional assays.** Flow cytometry was carried out by using LSR
438 Fortessa X-20 (BD) and cell sorting FACS Aria machines (BD). For apoptosis assay, 4×10^5 neutrophils
439 were stained with AnnexinV-FITC in Binding Buffer (Miltenyi Biotec). For mitochondria analyses,
440 MitoTracker™ Green and MitoTracker™ Red FM were added to neutrophils in MACS buffer for 15min
441 at RT (ThermoFisher Scientific). Alternatively, neutrophils were incubated with TMRM in RPMI for
442 20min at 37°C (Abcam). For phagocytosis assay, 10^5 neutrophils stimulated with zymosan-FITC
443 (50 μ g/ml, Fluorescein zymosanA BioParticles conjugates, FisherScientific), *C. albicans*-GFP (MOI1:1)
444 or *Escherichia coli*-GFP (MOI1:10) for 45min. Cells were stained with surface antibodies in MACS
445 buffer (Table S2).

446

447 **Endpoint dilution survival assay.** Isolated mouse neutrophils were seeded at 10^5 cells/well in 96-
448 well plates in RPMI+2% FBS and infected with *C. albicans* (serial fourfold dilutions of an OD=1
449 solution were added by rows (row1, MOI20:1; row2, MOI5:1...). After 24h at 37°C, colonies were
450 visualized with a Nikon TMS inverted microscope and counted at the lowest dilutions (row7-8).

451

452 **Killing assay.** Purified neutrophils were seeded in 96-well plate at 10^6 cells/well and stimulated with
453 PBS, *C. albicans* (MOI1) or *E. coli* (MOI10) for 90min at 37°C. Cells were washed and lysed with
454 200 μ l TritonX100 0.025%. Serial dilutions were plated on YEPD or LB plates.

455

456 **Oxydative burst.** Experiments were performed on a TriStar LB942 Reader using 10^5 neutrophils in
457 200 μ L HBSS (ThermoFisher Scientific) and luminol 80 μ M (Sigma) and stimulated with phorbol 12-
458 myristate 13-acetate (PMA; 0.1 μ g/mL; Sigma) or opsonized zymosan (20mg/mL zymosan A from
459 *Saccharomyces cerevisiae*; Sigma). The indexed maximal relative luminescence (in relative light units
460 [RLU]) was calculated as follow: indexed RLU max=(hemochromatosis patient maximal RLU)/[healthy
461 donor maximal RLU] \times 100. Alternatively, superoxyde dismutase (5Units/mL) and catalase A
462 (10Units/mL) were added to differentiate total and intracellular ROS production. Absorbance was
463 measured at 550nm for 30min.

464

465 **Real time bioenergetic profile analysis.** Mito Stress Test, Glycolytic Rate Assay and Real-time ATP
466 assay were performed on a XF96 Extracellular Flux Analyzer (Seahorse Biosciences). Mouse
467 neutrophils were seeded at 2×10^5 cells/well in RPMI+2%FBS in 0.01% poly-L-lysine pre-coated plate.
468 After 2h rest, cells were washed in Seahorse RPMI medium and incubated for 1h at 37°C without
469 CO₂. In the analyzer, oligomycin 1.5 μ M, FCCP 1 μ M, Rotenone+AntimycinA 0.5 μ M and 2DG 50 μ M
470 were injected at the indicated times. Protein standardization was performed after each experiment,
471 with no noticeable differences in protein concentration and cell phenotype.

472

473 **Electron microscopy.** Purified neutrophils were stimulated with *C. albicans* (MOI 2) or *E. coli* (MOI
474 10) for 1h at 37°C, washed in PBS and fixed. Samples preparation and SEM/TEM analyses were
475 performed at the Microscopy and Imaging Platform MIMA2 (Université Paris-Saclay, INRAE,
476 AgroParisTech, Jouy-en-Josas, France, <https://doi.org/10.15454/1.5572348210007727E12>).

477

478 **Proteomics.** 5 μ g protein extracts were submitted to in-gel digestion. Desalting was performed as
479 described before⁴⁹. Peptides were analyzed on a nanoElute-timsTOF ProLC-MS/MS system
480 (Bruker)⁵⁰. Raw files were analyzed using MaxQuant v1.6.10.43: database UP000000589_10090
481 (21994 entries, 17-Jun-2020). Data filtering, imputation and statistical analysis were performed with
482 ProStar Zero 1.20.0⁵⁰. Proteins with FDR<5% (Pounds method) were significant with a fold change
483 >1.2.

484

485 **Nuclear Magnetic Resonance.** 200µl culture media were analyzed by 1D 1H-NMR. All NMR spectra
486 were recorded on a Bruker AvanceIII 800MHz spectrometer equipped with a QPCI 5mm cryogenic
487 probe head. Spectra were acquired and processed using the Bruker Topspin 4.0 software.
488 Quantification of glucose and lactate was performed using addition of 25% TSPd4 in D2O as internal
489 standard.

490

491 **Statistical analysis.** Statistical analysis was performed using GraphPad Prism 7 software (see figure
492 legends).

493

494 **References**

- 495 1. Plichta DR, Graham DB, Subramanian S, et al. Therapeutic Opportunities in Inflammatory Bowel
496 Disease: Mechanistic Dissection of Host-Microbiome Relationships. *Cell* 2019;178:1041–1056.
- 497 2. Graham DB, Xavier RJ. Pathway paradigms revealed from the genetics of inflammatory bowel
498 disease. *Nature* 2020;578:527–539.
- 499 3. Dave M, Papadakis KA, Faubion WA. Immunology of Inflammatory Bowel Disease and
500 Molecular Targets for Biologics. *Gastroenterology Clinics of North America* 2014;43:405–424.
- 501 4. Wéra O, Lancellotti P, Oury C. The Dual Role of Neutrophils in Inflammatory Bowel Diseases.
502 *JCM* 2016;5:118.
- 503 5. Zhou GX, Liu ZJ. Potential roles of neutrophils in regulating intestinal mucosal inflammation of
504 inflammatory bowel disease: Role of neutrophils in IBD. *Journal of Digestive Diseases*
505 2017;18:495–503.
- 506 6. Caër C, Wick MJ. Human Intestinal Mononuclear Phagocytes in Health and Inflammatory Bowel
507 Disease. *Front Immunol* 2020;11:410.
- 508 7. Kolaczowska E, Kubes P. Neutrophil recruitment and function in health and inflammation. *Nat*
509 *Rev Immunol* 2013;13:159–175.
- 510 8. Segal AW. HOW NEUTROPHILS KILL MICROBES. *Annu Rev Immunol* 2005;23:197–223.
- 511 9. Mulholland MW, Delaney JP, Foker JE, et al. Gastrointestinal Complications of Congenital
512 Immunodeficiency States: *Annals of Surgery* 1983;198:673–680.
- 513 10. Segal AW. The NADPH oxidase and chronic granulomatous disease. *Molecular Medicine Today*
514 1996;2:129–135.
- 515 11. Annabi B, Mansfield BC, Hiraiwa H, et al. The Gene for Glycogen-Storage Disease Type 1b Maps
516 to Chromosome 11q23. *The American Journal of Human Genetics* 1998;62:400–405.
- 517 12. Uzel G, Tng E, Rosenzweig SD, et al. Reversion mutations in patients with leukocyte adhesion
518 deficiency type-1 (LAD-1). *Blood* 2008;111:209–218.

- 519 13. Bertin J, Guo Y, Wang L, et al. CARD9 Is a Novel Caspase Recruitment Domain-containing
520 Protein That Interacts With BCL10/CLAP and Activates NF- κ B. *Journal of Biological Chemistry*
521 2000;275:41082–41086.
- 522 14. Hsu Y-MS, Zhang Y, You Y, et al. The adaptor protein CARD9 is required for innate immune
523 responses to intracellular pathogens. *Nat Immunol* 2007;8:198–205.
- 524 15. Zhernakova A, Festen EM, Franke L, et al. Genetic Analysis of Innate Immunity in Crohn’s
525 Disease and Ulcerative Colitis Identifies Two Susceptibility Loci Harboring CARD9 and IL18RAP.
526 *The American Journal of Human Genetics* 2008;82:1202–1210.
- 527 16. Franke A, McGovern DPB, Barrett JC, et al. Genome-wide meta-analysis increases to 71 the
528 number of confirmed Crohn’s disease susceptibility loci. *Nat Genet* 2010;42:1118–1125.
- 529 17. Roth S, Ruland J. Caspase recruitment domain-containing protein 9 signaling in innate immunity
530 and inflammation. *Trends in Immunology* 2013;34:243–250.
- 531 18. McGovern DPB, Gardet A, Törkvist L, et al. Genome-wide association identifies multiple
532 ulcerative colitis susceptibility loci. *Nat Genet* 2010;42:332–337.
- 533 19. Strasser D, Neumann K, Bergmann H, et al. Syk Kinase-Coupled C-type Lectin Receptors Engage
534 Protein Kinase C- δ to Elicit Card9 Adaptor-Mediated Innate Immunity. *Immunity* 2012;36:32–
535 42.
- 536 20. Lanternier F, Mahdavian SA, Barbati E, et al. Inherited CARD9 deficiency in otherwise healthy
537 children and adults with *Candida* species–induced meningoencephalitis, colitis, or both. *Journal*
538 *of Allergy and Clinical Immunology* 2015;135:1558-1568.e2.
- 539 21. Cao Z, Conway KL, Heath RJ, et al. Ubiquitin Ligase TRIM62 Regulates CARD9-Mediated Anti-
540 fungal Immunity and Intestinal Inflammation. *Immunity* 2015;43:715–726.
- 541 22. LeibundGut-Landmann S, Groß O, Robinson MJ, et al. Syk- and CARD9-dependent coupling of
542 innate immunity to the induction of T helper cells that produce interleukin 17. *Nat Immunol*
543 2007;8:630–638.
- 544 23. Glocker E-O, Hennigs A, Nabavi M, et al. A Homozygous *CARD9* Mutation in a Family with
545 Susceptibility to Fungal Infections. *N Engl J Med* 2009;361:1727–1735.
- 546 24. Rieber N, Gazendam RP, Freeman AF, et al. Extrapulmonary *Aspergillus* infection in patients
547 with CARD9 deficiency. *JCI Insight* 2016;1. Available at:
548 <https://insight.jci.org/articles/view/89890> [Accessed June 15, 2021].
- 549 25. Sokol H, Conway KL, Zhang M, et al. Card9 Mediates Intestinal Epithelial Cell Restitution, T-
550 Helper 17 Responses, and Control of Bacterial Infection in Mice. *Gastroenterology*
551 2013;145:591-601.e3.
- 552 26. Lamas B, Richard ML, Leducq V, et al. CARD9 impacts colitis by altering gut microbiota
553 metabolism of tryptophan into aryl hydrocarbon receptor ligands. *Nat Med* 2016;22:598–605.
- 554 27. Hartjes L, Ruland J. CARD9 Signaling in Intestinal Immune Homeostasis and Oncogenesis. *Front*
555 *Immunol* 2019;10:419.

- 556 28. Hara H, Ishihara C, Takeuchi A, et al. The adaptor protein CARD9 is essential for the activation
557 of myeloid cells through ITAM-associated and Toll-like receptors. *Nat Immunol* 2007;8:619–
558 629.
- 559 29. Bergmann H, Roth S, Pechloff K, et al. Card9-dependent IL-1 β regulates IL-22 production from
560 group 3 innate lymphoid cells and promotes colitis-associated cancer. *Eur J Immunol*
561 2017;47:1342–1353.
- 562 30. Yang C-S, Rodgers M, Min C-K, et al. The Autophagy Regulator Rubicon Is a Feedback Inhibitor
563 of CARD9-Mediated Host Innate Immunity. *Cell Host & Microbe* 2012;11:277–289.
- 564 31. Gazendam RP, Geer A van de, Roos D, et al. How neutrophils kill fungi. *Immunol Rev*
565 2016;273:299–311.
- 566 32. Desai JV, Lionakis MS. The Role of Neutrophils in Host Defense Against Invasive Fungal
567 Infections. *Curr Clin Micro Rpt* 2018;5:181–189.
- 568 33. Drewniak A, Gazendam RP, Tool ATJ, et al. Invasive fungal infection and impaired neutrophil
569 killing in human CARD9 deficiency. *Blood* 2013;121:2385–2392.
- 570 34. Drummond RA, Collar AL, Swamydas M, et al. CARD9-Dependent Neutrophil Recruitment
571 Protects against Fungal Invasion of the Central Nervous System May RC, ed. *PLoS Pathog*
572 2015;11:e1005293.
- 573 35. Drummond RA, Swamydas M, Oikonomou V, et al. CARD9+ microglia promote antifungal
574 immunity via IL-1 β - and CXCL1-mediated neutrophil recruitment. *Nat Immunol* 2019;20:559–
575 570.
- 576 36. Loh JT, Xu S, Huo JX, et al. Dok3–protein phosphatase 1 interaction attenuates Card9 signaling
577 and neutrophil-dependent antifungal immunity. *Journal of Clinical Investigation*
578 2019;129:2717–2729.
- 579 37. Németh T, Futosi K, Sitaru C, et al. Neutrophil-specific deletion of the CARD9 gene expression
580 regulator suppresses autoantibody-induced inflammation in vivo. *Nat Commun* 2016;7:11004.
- 581 38. Tarte S, Gurung P, Samir P, et al. Cutting Edge: Dysregulated CARD9 Signaling in Neutrophils
582 Drives Inflammation in a Mouse Model of Neutrophilic Dermatoses. *Jl* 2018;201:1639–1644.
- 583 39. Kobayashi SD, Malachowa N, DeLeo FR. Influence of Microbes on Neutrophil Life and Death.
584 *Front Cell Infect Microbiol* 2017;7:159.
- 585 40. McCracken JM, Allen L-AH. Regulation of Human Neutrophil Apoptosis and Lifespan in Health
586 and Disease. *J Cell Death* 2014;7:JCD.S11038.
- 587 41. Li Y, Liang P, Jiang B, et al. CARD9 inhibits mitochondria-dependent apoptosis of
588 cardiomyocytes under oxidative stress via interacting with Apaf-1. *Free Radical Biology and*
589 *Medicine* 2019;141:172–181.
- 590 42. Burn GL, Foti A, Marsman G, et al. The Neutrophil. *Immunity* 2021;54:1377–1391.
- 591 43. Jun HS, Weinstein DA, Lee YM, et al. Molecular mechanisms of neutrophil dysfunction in
592 glycogen storage disease type Ib. *Blood* 2014;123:2843–2853.

- 593 44. Yamaguchi T, Ihara K, Matsumoto T, et al. Inflammatory Bowel Disease-Like Colitis in Glycogen
594 Storage Disease Type 1b: Inflammatory Bowel Diseases 2001;7:128–132.
- 595 45. Makowski L, Chaib M, Rathmell JC. Immunometabolism: From basic mechanisms to translation.
596 Immunol Rev 2020;295:5–14.
- 597 46. Németh T, Sperandio M, Mócsai A. Neutrophils as emerging therapeutic targets. Nat Rev Drug
598 Discov 2020;19:253–275.
- 599 47. Guidi L. Treatment of Crohn’s disease with colony-stimulating factors: An overview.
600 TCRM 2008;Volume 4:927–934.
- 601 48. Dupraz L, Magniez A, Rolhion N, et al. Gut microbiota-derived short-chain fatty acids regulate
602 IL-17 production by mouse and human intestinal $\gamma\delta$ T cells. Cell Reports 2021;36:109332.
- 603 49. Hamada S, Pionneau C, Parizot C, et al. In-depth proteomic analysis of *Plasmodium berghei*
604 sporozoites using trapped ion mobility spectrometry with parallel accumulation-serial
605 fragmentation. Proteomics 2021;21:2000305.
- 606 50. Pereira M, Richetta C, Sarango G, et al. *The Autophagy Receptor TAX1BP1 (T6BP) is a novel*
607 *player in antigen presentation by MHC-II molecules.* Immunology; 2021. Available at:
608 <http://biorxiv.org/lookup/doi/10.1101/2021.04.21.440798> [Accessed December 17, 2021].
- 609

610 **Main figure titles and legends**

611 **Figure 1. Lymphocytes have no intrinsic role in the *Card9*^{-/-} phenotype in colitis models.** (A)
612 Weight and (B) Disease Activity Index (DAI) score of DSS-exposed *Rag2*^{-/-} or *Rag2*^{-/-} x *Card9*^{-/-} mice.
613 (C) Colon length and (D) histological score of colon sections at day 7. Data points represent individual
614 mice. One representative experiment out of three. (E) Representative H&E-stained images of mid
615 colon cross-sections from DSS-exposed *Rag2*^{-/-} (left) and *Rag2*^{-/-} x *Card9*^{-/-} (right) mice at day 7. Scale
616 bars, 500 μm. (F) Weight of mice receiving naive T cells for adoptive transfer of colitis experiment.
617 *Rag2*^{-/-} received either WT or *Card9*^{-/-} lymphocytes. *Rag2*^{-/-} x *Card9*^{-/-} mice received WT lymphocytes.
618 Data are mean ± SEM of two independent experiments. *P<0.05, **P<0.01, ***P<0.001, ****P<0.0001
619 as determined by two-way analysis of variance (ANOVA) with Sidak's post-test (A, B, F) and Mann-
620 Whitney test (C, D). LT, lymphocytes T.

621 **Figure 2. *Card9* expression in neutrophils, but not in epithelial or CD11c⁺ cells, protects against**
622 **colitis.** (A) Weight and DAI score of DSS-exposed *Card9*^{Villin^{wt}} or *Card9*^{Villin^{cre}} mice. (B) Weight and
623 DAI score of DSS-exposed *Card9*^{cd11c^{wt}} or *Card9*^{cd11c^{cre}} mice. (C) Weight and DAI score of DSS-
624 exposed *Card9*^{Mrp8^{wt}} or *Card9*^{Mrp8^{cre}} mice. (D) Colon length, (E) histological score of colon sections and
625 (F) representative H&E-stained images of mid colon cross-sections from DSS-exposed *Card9*^{Mrp8^{wt}}
626 (left) and *Card9*^{Mrp8^{cre}} (right) mice at day 12. Scale bars, 500 μm. (G) Myeloperoxidase (MPO)
627 concentration in total colon tissue at day 12. (H) Lipocalin (*Lcn2*) expression by qRT-PCR in total
628 colon tissue at day 12, normalized to *Gapdh*. Data points represent individual mice. Data are mean ±
629 SEM of three independent experiments. *P<0.05, **P<0.01, ***P<0.001, ****P<0.0001 as determined
630 by two-way ANOVA with Sidak's post-test (A-C) and Mann-Whitney test (D-H).

631 **Figure 3. *Card9* deletion affects the number of neutrophils in the inflamed colon.** (A) Relative
632 expression of *Lcn2*, *Cxcr2* and *S1008a* in distal colon tissue of C57BL/6 WT mice during a DSS colitis
633 model relative to *Gapdh*. (B) Representative H&E-stained images of mid colon cross-sections from
634 DSS-exposed WT mice at day 0, 4, 7, 9, 12 and 16 after DSS exposure. Scale bars, 50 μm. (C) *Lcn2*,
635 *Cxcr2* and *S100A8* expression in total colon tissue from *Card9*^{Mrp8^{wt}} and *Card9*^{Mrp8^{cre}} mice at day 9 of
636 DSS colitis by qRT-PCR analyses, normalized to *Gapdh*. (D) Representative flow cytometry plots of
637 Ly6G⁺CD11b⁺ cells (neutrophils) in the colon lamina propria (LP) of DSS-exposed *Card9*^{Mrp8^{wt}} and
638 *Card9*^{Mrp8^{cre}} mice. (E) Percentage and count of Ly6G⁺CD11b⁺ cells in the LP of DSS-exposed

639 *Card9*^{Mrp8wt} and *Card9*^{Mrp8cre} mice. (F) Ly6G and (G) CD11b expression (MFI for Mean Fluorescence
640 Intensity) of Ly6G⁺CD11b⁺ neutrophils from *Card9*^{Mrp8wt} and *Card9*^{Mrp8cre} mice. Data points represent
641 individual mice. Data are mean ± SEM of two independent experiments. *P<0.05, **P<0.01,
642 ***P<0.001 as determined by Mann-Whitney tests.

643 **Figure 4. *C. albicans* killing capacity is impacted by *Card9* deletion in neutrophils.** (A)
644 Representative images of *C. albicans* cfu number at the endpoint dilution after infection of *Card9*^{WT},
645 *Card9*^{-/-}, *Card9*^{Mrp8wt} or *Card9*^{Mrp8cre} neutrophils for 24h, using a microscope (top) or directly showing *C.*
646 *albicans* cfu in the 96-well plate, with a photography from above (middle picture) or a scan from below
647 the plate (bottom picture). (B) *C. albicans* cfu after infection of neutrophils for 24h. CfU counting was
648 performed in 96 well plates using a microscope. Data points represent individual mice. Data are mean
649 ± SEM of three independent experiments. (C) *C. albicans* cfu number after infection of *Card9*^{Mrp8wt} or
650 *Card9*^{Mrp8cre} neutrophils for 3 or 24h. CfU counting was performed after plating on YEPD agar plates.
651 Data are mean ± SEM of two independent experiments. (D) Experimental design of antibiotic
652 treatments and *C. albicans* inoculation in mice treated with 3% DSS. (E) Weight, (F) DAI and (G) colon
653 length of DSS-exposed *Card9*^{Mrp8wt} and *Card9*^{Mrp8cre} mice after colonization with *C. albicans*. (H-K)
654 Fungal burden in the feces (H), caecal content (I), caecal and colon tissue (J) and liver, spleen and
655 kidney (K) of DSS-exposed *Card9*^{Mrp8wt} and *Card9*^{Mrp8cre} mice after colonization with *C. albicans*. Data
656 are mean ± SEM of two independent experiments. *P<0.05, **P<0.01, ***P<0.001, ****P<0.0001 as
657 determined by one-way ANOVA with Tukey's post-test (A), two-way ANOVA with Sidak's post-test (E,
658 F) and Mann-Whitney test (C, G, I-K). Genta, gentamycin.

659 **Figure 5. The absence of *Card9* impacts neutrophils survival by increasing apoptosis.** (A)
660 Representative flow cytometry plots of Ly6G⁺CD11b⁺ neutrophils purified from bone marrow of
661 *Card9*^{Mrp8wt} (left) and *Card9*^{Mrp8cre} (right) mice, co-stained with AnnexinV and a Live/Dead marker. (B)
662 AnnexinV MFI of Ly6G⁺CD11b⁺ neutrophils from *Card9*^{Mrp8wt} and *Card9*^{Mrp8cre} mice, incubated for 1h at
663 37°C. (C) Percentage of apoptotic neutrophils (Q1: AnnexinV⁺LD⁻ cells), dead (late apoptotic/necrotic)
664 neutrophils (Q2: AnnexinV⁺LD⁺ cells) and viable neutrophils (Q4: AnnexinV⁻LD⁻ cells) amongst the
665 Ly6G⁺CD11b⁺ population. (D) Percentage of CD62L⁺ and CD62L⁻ neutrophils amongst the
666 Ly6G⁺CD11b⁺ population. Data represent one out of two independent experiments. (E) Histogram
667 representing Gene Ontology biological processes significantly enriched amongst proteins down- (blue)

668 or up-regulated (red) in *Card9*^{Mrp8cre} compared to *Card9*^{Mrp8wt} neutrophils in the unstimulated condition.
669 (F) Morpheus heat-map representing mitochondria-related proteins significantly down- or up-regulated
670 in *Card9*^{Mrp8cre} compared to *Card9*^{Mrp8wt} neutrophils in the unstimulated condition. E and F obtained
671 from proteomics data analysis. *P<0.05, **P<0.01, ***P<0.001, ****P<0.0001 as determined by Mann-
672 Whitney test (B) and two-way ANOVA with Sidak's post-test (C-D).

673 **Figure 6. *Card9* controls neutrophil energetic metabolism by affecting mitochondrial function.**

674 (A) Representative flow cytometry plots and percentages of MitoGreen⁺MitoRed⁻ cells (corresponding
675 to cells with dysfunctional mitochondria) amongst Ly6G⁺CD11b⁺ neutrophils. Neutrophils were purified
676 from the bone marrow of *Card9*^{Mrp8wt} or *Card9*^{Mrp8cre} mice, and incubated for 1h at 37°C. (B)
677 Representative flow cytometry plots and percentages of TMRM⁻ cells (corresponding to cells with
678 dysfunctional mitochondria/apoptotic or metabolically inactive cells) amongst Ly6G⁺CD11b⁺
679 neutrophils. (C) Oxygen Consumption Rate (OCR) of *Card9*^{Mrp8wt} and *Card9*^{Mrp8cre} neutrophils
680 measured during a Seahorse Cell Mito Stress assay. (D) Basal respiration (late rate measurement
681 before oligomycin injection (t3) - non-mitochondrial respiration rate (t12)) and ATP production rate
682 (late rate measurement before oligomycin (ATP synthase blocker) injection (t3) – minimum rate
683 measurement after oligomycin injection (t6) obtained from the Seahorse Cell Mito Stress assay. (E)
684 ATP rate index and energetic map of *Card9*^{Mrp8wt} and *Card9*^{Mrp8cre} neutrophils obtained from the
685 Seahorse Real-time ATP rate assay. (F) Percentage of apoptotic cells amongst the Ly6G⁺CD11b⁺
686 neutrophil population of *Card9*^{Mrp8wt} and *Card9*^{Mrp8cre} genotypes after treatment with 2-DG 10 mM or
687 (G) oligomycin 1.5 μM for 1h. (H) Percentage of apoptotic and necrotic cells amongst the
688 Ly6G⁺CD11b⁺ neutrophil population of *Card9*^{Mrp8wt} and *Card9*^{Mrp8cre} genotypes after addition of H2O2
689 0.01 mM for 1h to increase oxydative stress. Data are mean ± SEM of at least two independent
690 experiments. *P<0.05, **P<0.01, ***P<0.001, ****P<0.0001 as determined by Mann-Whitney test (A,
691 B, D, E, F) or two-way ANOVA with Sidak's post-test (G, H). Norm. Unit, normalized unit; FCCP,
692 Carbonyl cyanide 4-(trifluoromethoxy)phenylhydrazone; Rot/AA, Rotenone/AntimycinA; 2DG, 2 deoxy-
693 glucose; OligoA, oligomycinA.

694

695 **Supplemental Figure and Table**

696 **Figure S1. *Card9* is mainly expressed by myeloid cells.** (A) *Card9* expression in different organs of
697 *Card9*^{WT} and *Card9*^{-/-} mice by quantitative RT-PCR analyses, normalized to *Gapdh*. (B) CARD9 and
698 β-ACTIN expression in different organs of *Card9*^{WT} and *Card9*^{-/-} mice by Western Blot analyses. (C)
699 *Card9* expression in different sorted cell populations from the spleen and bone marrow of *Card9*^{WT}
700 and *Card9*^{-/-} mice by quantitative RT-PCR analyses, normalized to *Gapdh*.

701 **Figure S2. Validation of conditional knockout mice strains.** (A) *Card9* expression in colonic
702 epithelial cells and tissue from *Card9*^{Villin^{wt}} and *Card9*^{Villin^{cre}} mice (up right panel), CD11c⁺ purified cells
703 and CD11c⁻ fraction from the spleen of *Card9*^{Cd11c^{wt}} and *Card9*^{Cd11c^{cre}} mice (up left panel) and Ly6G⁺
704 purified neutrophils and Ly6G⁻ fraction from the bone marrow of *Card9*^{WT}, *Card9*^{-/-}, *Card9*^{Mrp8^{wt}} and
705 *Card9*^{Mrp8^{cre}} mice (lower panels) by qRT-PCR analyses, normalized to *Gapdh*. (B) CARD9 and β-
706 ACTIN expression in Ly6G⁺ purified neutrophils and Ly6G⁻ fraction from the bone marrow of *Card9*^{WT},
707 *Card9*^{-/-}, *Card9*^{Mrp8^{wt}} and *Card9*^{Mrp8^{cre}} mice by Western blot. (C) Flow cytometry plots representing total
708 cell populations of the bone marrow of a C57BL/6 mouse (left panel), and Ly6G⁺CD11b⁺ neutrophils
709 purified from the bone marrow using Ly6G ultrapure magnetic beads and MACS column (right panel).
710 (D) Colon length of DSS-exposed *Card9*^{Villin^{wt}}, *Card9*^{Villin^{cre}}, *Card9*^{Cd11c^{wt}} and *Card9*^{Cd11c^{cre}} mice. (E)
711 AhR activity of feces from *Card9*^{Mrp8^{wt}} and *Card9*^{Mrp8^{cre}} mice at steady-state, using HepG2 reporting
712 cells. (F) Weight and DAI score of DSS-exposed *Card9*^{Mrp8^{wt}} or *Card9*^{Mrp8^{cre}} mice for 9 days.

713 **Figure S3. Imaging of *Card9*-deleted neutrophils.** (A) Immunofluorescence staining of *Card9*^{WT},
714 *Card9*^{-/-}, *Card9*^{Mrp8^{wt}} and *Card9*^{Mrp8^{cre}} neutrophils unstimulated or stimulated with zymosan for 1 or 3h.
715 Blue for DNA, red for β-ACTIN. Scale bars, 5 μm. (B) Scanning electron microscopy (SEM, left) or
716 Transmission electron microscopy (TEM, right) of *Card9*^{Mrp8^{wt}} and *Card9*^{Mrp8^{cre}} neutrophils
717 unstimulated or stimulated with *C. albicans* or *E. coli* for 1h. White arrows point *C. albicans* or *E. coli*
718 phagocytosed by neutrophils. Scale bars, 1 or 1.5 μm.

719 **Figure S4. *C. albicans* killing capacity is impacted by *Card9* deletion in neutrophils, but not
720 phagocytosis capacity, ROS production or autophagy.** (A) Representative flow cytometry plots
721 showing percentages of Ly6G⁺FITC⁺ and Ly6G⁺GFP⁺ *Card9*^{WT} or *Card9*^{-/-} neutrophils stimulated by
722 zymosan-FITC (50μg/ml, Fluorescein zymosan A BioParticles conjugates), *C. albicans*-GFP (MOI 1:1)
723 or *E. coli*-GFP (MOI 1:10) for 45 min. (B) Graph representing phagocytosis rates obtained by flow

724 cytometry analysis. (C-D) Oxydative burst kinetics of *Card9*^{WT}, *Card9*^{-/-}, *Card9*^{Mrp8^{wt}} and *Card9*^{Mrp8^{cre}}
725 neutrophils as measured by luminol-amplified chemiluminescence of *Card9*^{WT} and *Card9*^{-/-} (left
726 panel) and *Card9*^{Mrp8^{wt}} and *Card9*^{Mrp8^{cre}} (right panel) neutrophils after stimulation with (C) PMA
727 (phorbol 12-myristate 13-acetate; 0.1 µg/mL; Sigma) or (D) opsonized zymosan (20 mg/mL, zymosan
728 A from *Saccharomyces cerevisiae* opsonized with 10% SVF). (E) Total and Intracellular Reactive
729 Oxygen Species (ROS) produced by *Card9*^{WT} and *Card9*^{-/-} neutrophils (left), or *Card9*^{Mrp8^{wt}} and
730 *Card9*^{Mrp8^{cre}} neutrophils (right) in unstimulated condition or after 90 min stimulation with non-opsonized
731 zymosan (0.5 mg/mL). RLU, relative light unit. (F) Western blot showing p62 (62 KDa) and
732 LC3BI/LC3BII (16 and 14 KDa) autophagy proteins in *Card9*^{WT}, *Card9*^{-/-}, *Card9*^{Mrp8^{wt}} and *Card9*^{Mrp8^{cre}}
733 neutrophils purified from the bone marrow and incubated 1h in RPMI +2% FBS at 37°C. (G)
734 Fungi/bacteria loads in feces from *Card9*^{Mrp8^{wt}} or *Card9*^{Mrp8^{cre}} mice during DSS colitis measured by
735 qRT-PCR (ratio of 2^{-C_t}).

736 **Figure S5. The absence of *Card9* impacts neutrophils survival by increasing apoptosis.** (A)
737 Representative flow cytometry plots of Ly6G⁺CD11b⁺ neutrophils purified from bone marrow of
738 *Card9*^{WT} (left) and *Card9*^{-/-} (right) mice, co-stained with AnnexinV and a Live/Dead marker. (B)
739 AnnexinV MFI of Ly6G⁺CD11b⁺ neutrophils from *Card9*^{WT} and *Card9*^{-/-} mice, incubated for 1h at
740 37°C. (C) Percentage of apoptotic neutrophils (Q1: AnnexinV⁺LD⁻ cells), dead (late apoptotic/necrotic)
741 neutrophils (Q2: AnnexinV⁺LD⁺ cells) and viable neutrophils (Q4: AnnexinV⁻LD⁻ cells) amongst the
742 Ly6G⁺CD11b⁺ population. (D) Percentage of CD62L⁺ and CD62L⁻ neutrophils amongst the
743 Ly6G⁺CD11b⁺ population. Data represent one out of two independent experiments. *P<0.05, **P<0.01,
744 ***P<0.001, ****P<0.0001 as determined by Mann-Whitney test (B) or two-way ANOVA with Sidak's
745 post-test (C-D).

746 **Figure S6. *Card9* controls neutrophil energetic metabolism by affecting mitochondrial function.**
747 (A) Extracellular Acidification Rate (ECAR) of *Card9*^{Mrp8^{wt}} and *Card9*^{Mrp8^{cre}} neutrophils measured
748 during a Seahorse Glycolytic rate assay in unstimulated condition (RPMI + 2% FBS). Graph
749 represents basal glycolysis (t2). (B) Lactate/glucose ratio in 24h culture supernatant of *Card9*^{Mrp8^{wt}} and
750 *Card9*^{Mrp8^{cre}} neutrophils measured by metabolomics data analyses. (C) Representative flow cytometry
751 plots and percentages of MitoGreen⁺MitoRed⁻ cells (corresponding to cells with dysfunctional
752 mitochondria) amongst the Ly6G⁺CD11b⁺ neutrophil population from *Card9*^{WT} or *Card9*^{-/-} mice

753 incubated for 1h at 37°C. (D) Representative flow cytometry plots and percentages of TMRM⁻ cells
754 (corresponding to cells with dysfunctional mitochondria/apoptotic or metabolically inactive cells)
755 amongst the Ly6G⁺CD11b⁺ neutrophil population incubated for 3h at 37°C. (E) Oxygen Consumption
756 Rate (OCR) and Extracellular Acidification Rate (ECAR) of *Card9*^{WT} or *Card9*^{-/-} neutrophils measured
757 during a Seahorse Cell Mito Stress assay or a Seahorse Glycolytic rate assay, respectively. Data are
758 mean ± SEM of at least two independent experiments. *P<0.05, **P<0.01, ***P<0.001, ****P<0.0001
759 as determined by Mann-Whitney tests. FCCP, Carbonyl cyanide 4-(trifluoromethoxy)phenylhydrazone;
760 Rot/AA, Rotenone/AntimycinA; 2-DG, 2-deoxy-D-glucose.

761 **Table S1. Histological grading of colitis**

762 **Table S2. List of oligonucleotides and antibodies**

763

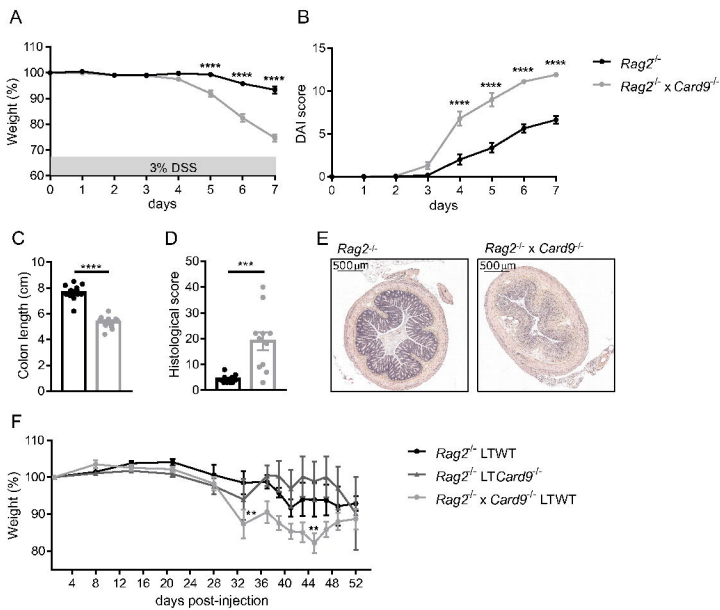


Figure 1

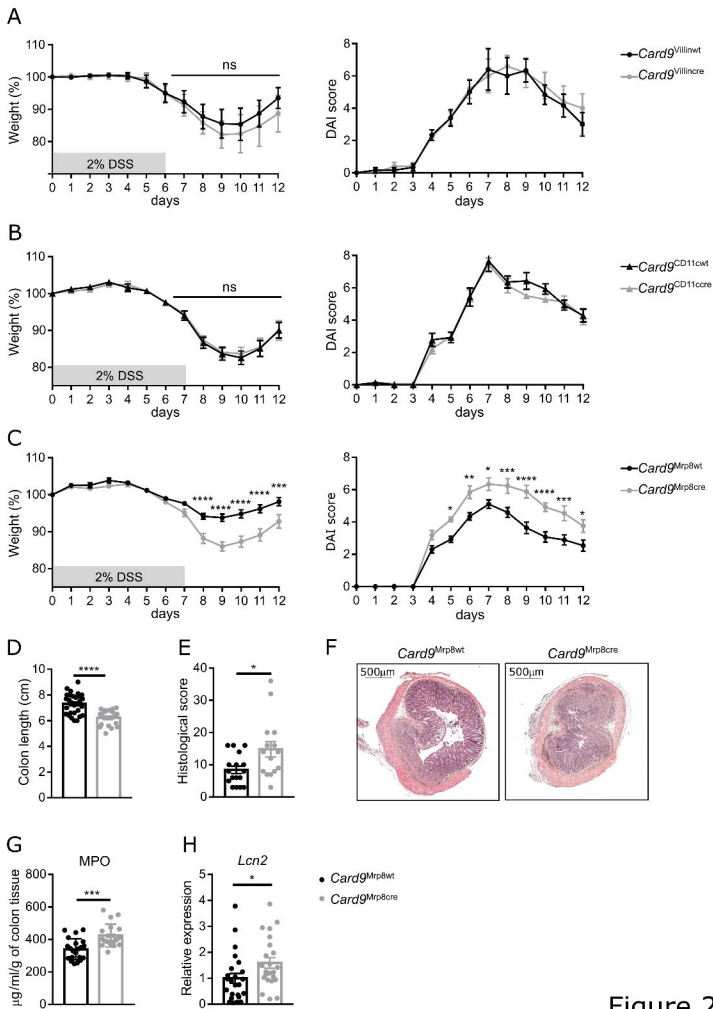


Figure 2

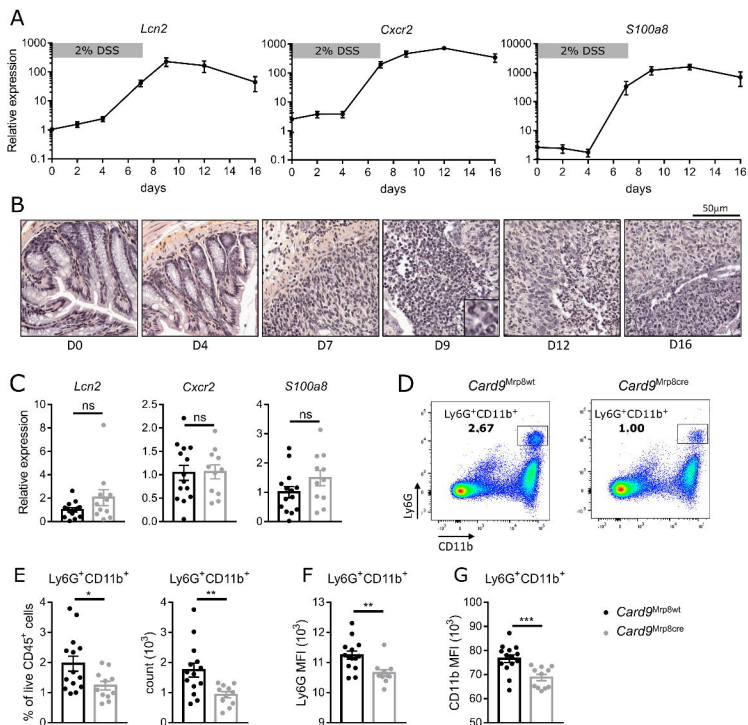


Figure 3

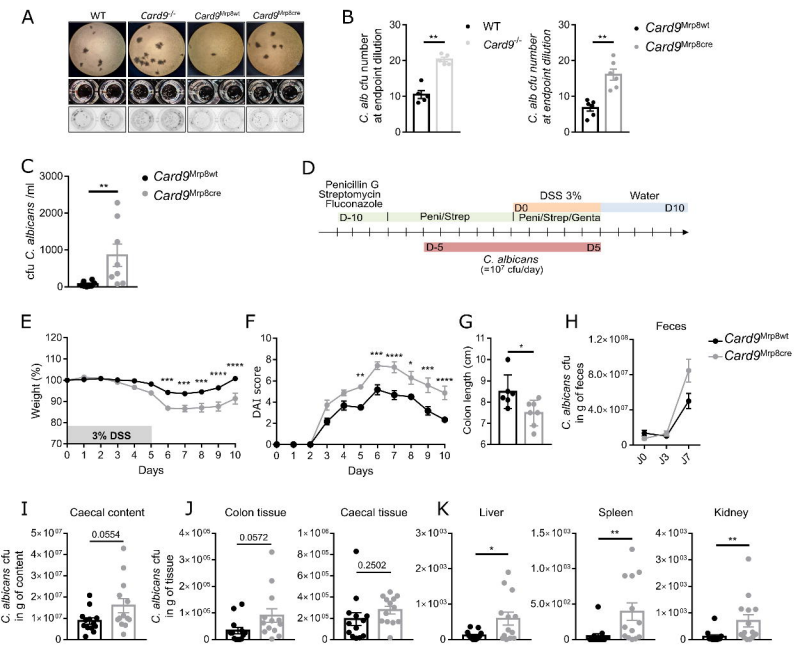


Figure 4

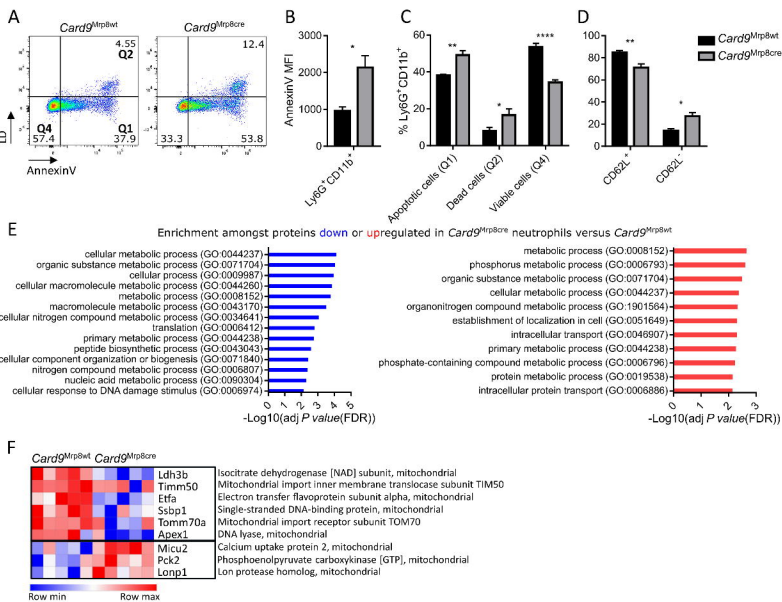


Figure 5

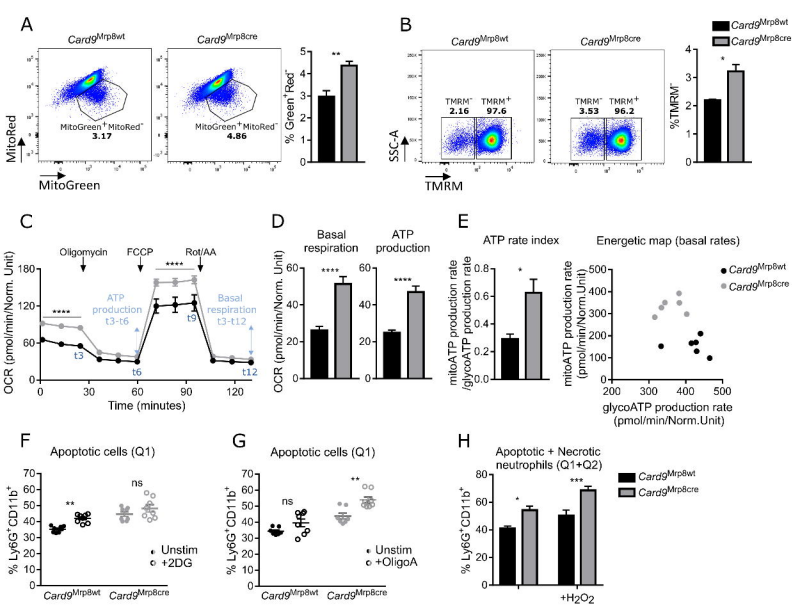


Figure 6